doi:10.1038/nature23462

Ram-pressure feeding of supermassive black holes

Bianca M. Poggianti[1], Yara L. Jaffé[2], Alessia Moretti[1], Marco Gullieuszik[1], Mario Radovich[1], Stephanie Tonnesen[3], Jacopo Fritz[4], Daniela Bettoni[1], Benedetta Vulcani[1,5], Giovanni Fasano[1], Callum Bellhouse[2,6], George Hau[2] & Alessandro Omizzolo[7]

When a supermassive black hole at the centre of a galaxy accretes matter, it gives rise to a highly energetic phenomenon: an active galactic nucleus[1,2]. Numerous physical processes have been proposed to account for the funnelling of gas towards the galactic centre to feed the black hole. There are also several physical processes that can remove gas from a galaxy[3], one of which is ram-pressure stripping by the hot gas that fills the space between galaxies in galaxy clusters[4]. Here we report that six out of a sample of seven 'jellyfish' galaxies—galaxies with long 'tentacles' of material that extend for dozens of kiloparsecs beyond the galactic disks[5,6]—host an active nucleus, and two of them also have galactic-scale ionization cones. The high incidence of nuclear activity among heavily stripped jellyfish galaxies may be due to ram pressure causing gas to flow towards the centre and triggering the activity, or to an enhancement of the stripping caused by energy injection from the active nucleus, or both. Our analysis of the galactic position and velocity relative to the cluster strongly supports the first hypothesis, and puts forward ram pressure as another possible mechanism for feeding the central supermassive black hole with gas.

Black holes of different sizes are very common in the Universe. It is now well established that most, if not all, galaxies host at their centre a supermassive black hole of a few million to a few billion solar masses[7,8]. When a black hole accretes matter, it converts the gravitational energy of the accreted matter into mechanical and electromagnetic energy, giving rise to some of the most energetic astrophysical phenomena, namely active galactic nucleus (AGN).

One of the central questions regarding AGN is why if supermassive black holes are present in most galaxies, only a small fraction of these are AGN, that is, why only a few of them are accreting matter. It is believed that the black hole growth must be episodic, last typically 10^7–10^8 yr and that it must be related to a mechanism that drives gas to the galaxy centre efficiently. Major mergers of two galaxies are among the best candidates for the most luminous AGN[9], while galaxy internal instabilities (for example, driven by galaxy bars) or fast tidal encounters between galaxies might account for less luminous systems[10,11].

A prerequisite for AGN activity is therefore the availability of gas in the galaxy disk to feed the black hole. In the current cosmological paradigm, the interstellar medium present in the galaxy disk gets consumed by the formation of new stars but is continuously replenished by the cooling of hot gas present in the galaxy dark matter halo[12]. However, there are several physical processes that can remove gas from galaxies, especially in dense environments such as galaxy clusters and groups[3]. Ram-pressure stripping due to the pressure exerted by the intergalactic medium on the galaxy interstellar medium is considered the most efficient of such processes[4]. The galaxy loses its gas because the ram pressure overcomes the local binding energy, and in those regions of the galaxy where gas is removed, the formation of new stars is inhibited. However, before quenching the star formation, ram pressure can produce an enhancement of the star-formation rate, as thermal instabilities and turbulent motions provoke the collapse of molecular clouds[13,14].

The most spectacular examples of galaxies undergoing gas stripping by ram pressure are the 'jellyfish' galaxies, whose 'tentacles' are formed of stripped gas and newly born stars[5,6]. In this work, we show that there is a close link between strong ram pressure and AGN activity in jellyfish galaxies, establishing for the first time a probable causal connection between the two phenomena. Our findings are based on results from GASP (GAs Stripping Phenomena in galaxies with MUSE[15], http://web.oapd.inaf.it/gasp), which is an ESO Large Program aimed at studying where, how and why gas can get removed from galaxies. GASP studies 94 galaxies at redshifts $z = 0.04$–0.07 that occur in clusters, groups and the general field, and have been selected from optical images to have unilateral debris and asymmetric morphologies, suggestive of gas-only removal mechanisms. Spatially resolved gas and stellar kinematics and physical properties are obtained with the MUSE spectrograph on the Very Large Telescope.

For the present work, we have selected all the cluster jellyfish galaxies observed so far by GASP which have striking tentacles of ionized gas, as seen by MUSE in the Hα line in emission at 6,563 Å. We have selected those galaxies whose Hα tentacles are at least as long as the galaxy stellar disk diameter (see Extended Data Table 1). These are all massive galaxies, with stellar masses in the range $(0.4$–$3) \times 10^{11}$ solar masses, $M_{\odot}$.

The Hα velocity maps of the seven galaxies selected are shown in Fig. 1b, c and 2b and are contrasted with the corresponding stellar velocity maps (in Figs 1a and 2a). These figures illustrate the long extraplanar ionized gas tentacles extending out to about 20–100 kpc. In contrast to the Hα velocity maps, the stellar velocity field is regular and shows that the stellar kinematics are undisturbed by the force acting on the gas. The comparison between the gaseous and stellar morphologies and velocity maps shows that these galaxies are undergoing a gas-only removal mechanism due to the impact of the intracluster medium (ICM) such as ram-pressure stripping. Ram-pressure calculations supporting this hypothesis for some of these galaxies are presented in the individual galaxy studies[15–17].

The main result is shown in Fig. 3. We use standard diagnostic diagrams of emission-line ratios to assess the mechanism responsible for the gas ionization. The gas emitting in Hα can be ionized by different mechanisms (see the keys in Fig. 3): by photons from young hot stars ('star-forming'), by the central AGN ('AGN'), by a combination of the two ('composite') or by 'low ionization nuclear emission-line regions' ('LINERs') that might be due to a low-luminosity AGN or other mechanisms such as shocks or old stars. To discriminate between these ionization mechanisms, we use in our diagnostic diagrams a classification proposed elsewhere[18–21].

According to the MUSE line ratios, the galaxy central regions are powered by AGN emission in JO201, JO204, JW100, JO206 and JO135. In JO194, the central emission is LINER-like, as it is in a slightly larger annular region surrounding a star-formation-dominated ring. In contrast, line ratios in JO175 are consistent with photoionization by star formation in the centre and throughout most of the disk and tentacles.

[1]INAF–Astronomical Observatory of Padova, vicolo dell'Osservatorio 5, 35122 Padova, Italy. [2]European Southern Observatory, Alonso de Cordova 3107, Vitacura, Casilla 19001, Santiago de Chile, Chile. [3]Carnegie Observatory, 813 Santa Barbara Street, Pasadena, California 91101, USA. [4]Instituto de Radioastronomia y Astrofisica, UNAM, Campus Morelia, AP 3-72, CP 58089, Mexico. [5]School of Physics, The University of Melbourne, Swanston Street and Tin Alley, Parkville, Victoria 3010, Australia. [6]University of Birmingham, School of Physics and Astronomy, Edgbaston, Birmingham, UK. [7]Vatican Observatory, Vatican City.

© 2017 Macmillan Publishers Limited, part of Springer Nature. All rights reserved.

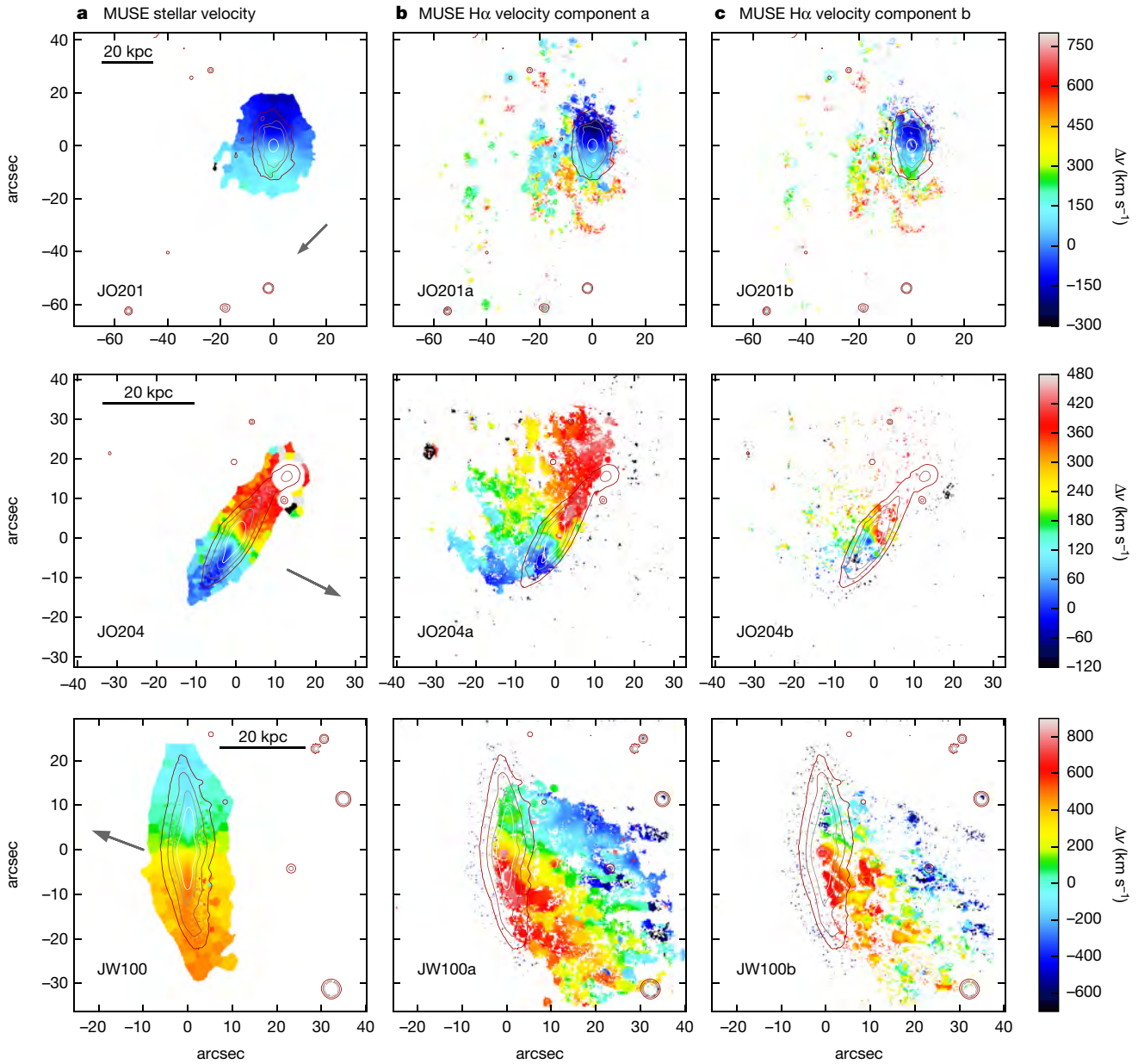

Figure 1 | MUSE stellar velocity maps and Hα maps for JO201, JO204 and JW100. Shown are MUSE stellar velocity maps (**a**; left column) and Hα velocity maps (**b** and **c**, respectively middle and right column) of our jellyfish galaxies. JO201, JO204 and JW100 have regions with two line components separated in velocity (for example, JO201a and JO201b), and their gas velocity maps are plotted separately (in **b** and **c**). Contours in all panels are stellar isophotes (Methods) and indicate where the galaxy stellar disk is. In the leftmost column, the scale in kpc is indicated by a bar and the arrow points in the direction of the cluster centre. North is up and east is left.

Thus, the great majority (5/7) of our jellyfish galaxies host an AGN that is evident from the MUSE spectra. This is at odds with the fact that only 3% of emission-line galaxies with a spectroscopic classification in clusters at low redshift show evidence for AGN activity[22] (this fraction is only slightly higher, about 8%, among field galaxies[23]). The AGN in our galaxies are responsible for the ionization in a central region that is generally quite extended, up to 10 kpc in diameter (for example, JO201, Fig. 3).

Three of our galaxies (JO201, JO204, JW100) have two spectral components with different velocities. The two components correspond to gas at different velocities that are seen in projection along the line of sight. Interestingly, the two components in JO201 are both powered by the AGN in the central region, while the two components of JO204 have a quite different spatial distribution: whereas the second component is AGN-dominated in the central region, the first component (JO204a) has an AGN-powered extraplanar region, extending up to 15 kpc away from the stellar isophotes (Methods), that appears to be an AGN ionization cone along the tentacles. Similarly, regions illuminated by the AGN are seen out to large galactocentric distances in the disk of JO135, and to 6 kpc in projection outside the stellar disk to the north. Therefore, JO204 and JO135 possess a galaxy-scale ionization cone powered by the AGN.

The case of JO194 is more doubtful, as the LINER-like emission can be due either to a low-luminosity AGN or to other sources of ionization. The spatial distribution of the LINER-like emission favours an AGN origin. Chandra (0.3–8 keV) X-ray luminosities (L_X; Extended Data Table 1) support our MUSE findings of AGN in JO194 as well as in JO135, JW100, JO201 and JO206, the last two being very X-ray-luminous sources with $L_X = 7.3 \times 10^{41}$ erg s^{-1} and $L_X = 7.7 \times 10^{42}$ erg s^{-1}, respectively. An independent

© 2017 Macmillan Publishers Limited, part of Springer Nature. All rights reserved.

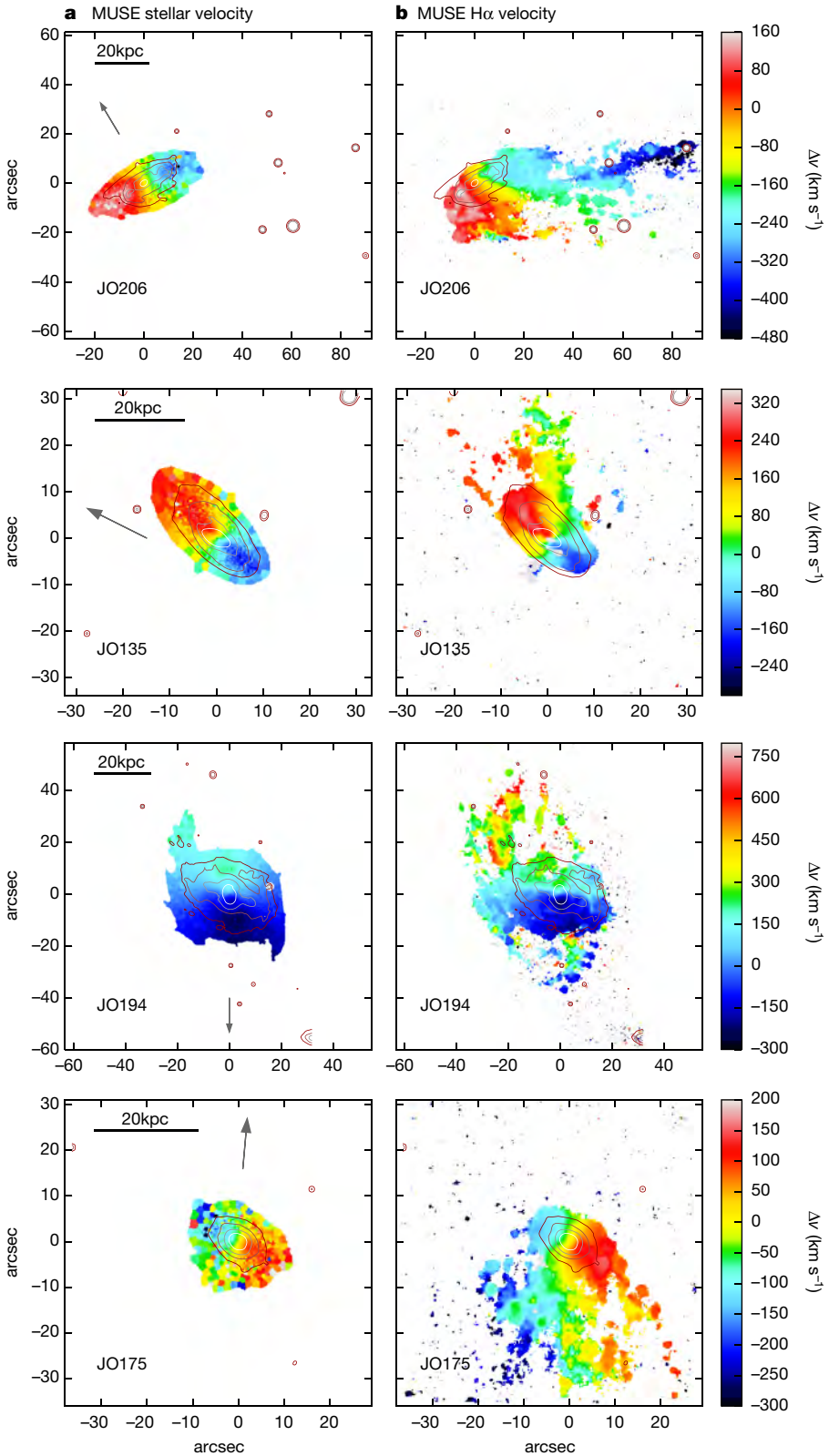

Figure 2 | MUSE stellar velocity map and Hα map for JO206, JO135, JO194 and JO175. As Fig. 1 for the other four galaxies, but with a single column of Hα velocities.

proxy for the AGN luminosities are the luminosities of [O III] at 5,007 Å (that is, [O III]5,007), listed in Extended Data Table 1. The conclusion that AGN emission is widespread in our jellyfish sample is further reinforced in the summary diagram in Extended Data Fig. 1.

The high incidence of AGN among the most striking jellyfish galaxies uncovers a link between nuclear activity and strong ram-pressure stripping. Two scenarios can be envisaged. In the first scenario, the ram pressure is capable of funnelling the gas towards the galaxy centre, causing gas accretion onto the central black hole and triggering the

© 2017 Macmillan Publishers Limited, part of Springer Nature. All rights reserved.

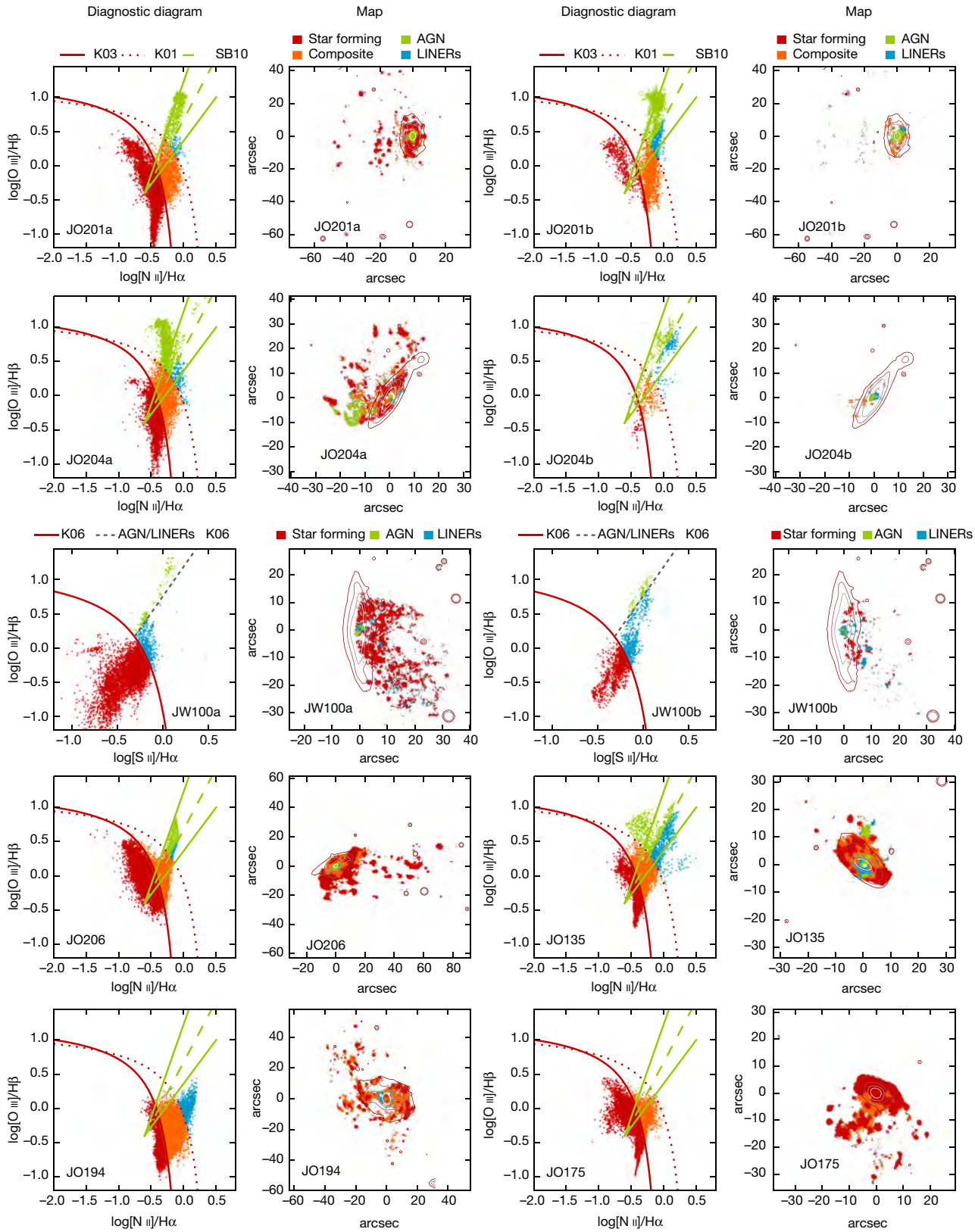

Figure 3 | Diagnostic diagrams and maps for all jellyfish galaxies. Shown are spatially resolved diagnostic diagrams (columns 1 and 3) and maps (columns 2 and 4) for all MUSE pixels where lines are measured with a signal-to-noise ratio of >3. For JO201, JO204 and JW100 the two components are presented separately and there are four panels per galaxy. In the diagnostic diagrams, lines[18–20] separate regions of different ionization mechanisms: star-forming, H II-AGN composite, AGN and LINERs (see main text and Methods for details). In the case of JW100 only, lines[21] separate star-forming, AGN and LINERs regions. In the keys, K01 indicates ref. 18; K03, ref. 19; SB10, ref. 20; K06, ref. 21. Contours are stellar isophotes, as in Fig. 1. For each galaxy we have inspected both the [O III]5,007/Hβ versus [N II]6,583/Hα and the [O III]/Hβ versus [S II]6,717/Hα diagrams and found no discrepancy of classification between the two. For convenience, we show only the spatially resolved [N II]6,583/Hα plot for each galaxy, except for JW100 for which we use the [S II]6,717/Hα plot instead, because at the JW100 redshift the [N II] line is contaminated by a sky line.

© 2017 Macmillan Publishers Limited, part of Springer Nature. All rights reserved.

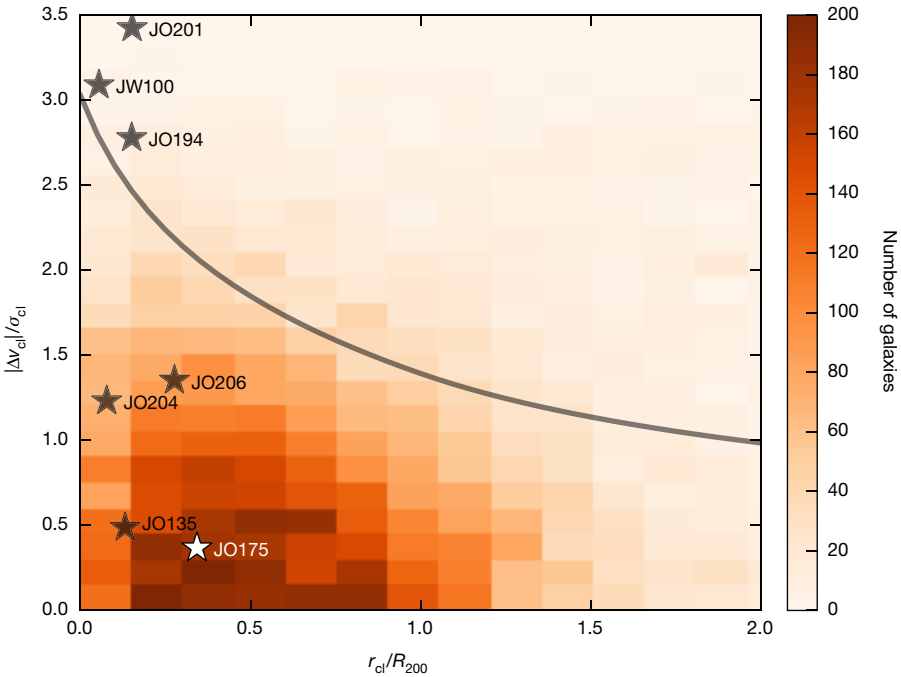

Figure 4 | Differential velocity versus cluster-centric distance. In this phase-space diagram, we show projected differential velocity Δv_{cl} with respect to the cluster median velocity, normalized by the cluster velocity dispersion σ_{cl}, versus the projected cluster-centric distance r_{cl}, in units of cluster virial radius R_{200}. The latter is defined as the projected radius delimiting a sphere with interior mean density 200 times the critical density of the Universe. In this diagram, velocities and radii are lower limits to the three-dimensional velocity of the galaxy through the ICM and cluster-centric distance, respectively. The locations of our jellyfish galaxies are shown by the star plotting symbols. The only jellyfish galaxy with no AGN, JO175, is marked with a white star. The number density of all cluster galaxies from the OmegaWINGS sample at each location in the diagram is colour coded (bar on right-hand side). The darker orange regions trace the locations of the oldest cluster members, located near the cluster core (at low r_{cl}/R_{200} and $|\Delta v_{cl}|/\sigma_{cl}$) after having settled into the potential well. Thus, the position of the jellyfish galaxies in phase-space implies that they are being stripped on first infall onto the cluster. The curve represents the escape velocity in a dark matter halo[30].

activity. Hydrodynamic simulations have found that when galactic gas interacts with the non-rotating ICM it can lose angular momentum and spiral into the central region of a galaxy[24–26]. Another possible method by which ram-pressure stripping could feed an AGN is inflow of gas towards the galactic centre generated by oblique shocks in a disk that is flared due to the magnetic field[27].

The second scenario sees the AGN as injecting a large amount of energy into the interstellar medium, thus decreasing its binding energy and making it more easily stripped, or even directly ejecting it from the galaxy[28]. In this case, the AGN feedback—the energy injected into the interstellar medium—would increase the efficiency of ram pressure, and is an important component producing the striking jellyfish appearance.

To discriminate between these two hypotheses, we show in Fig. 4 the location of our jellyfish galaxies in a projected position versus velocity phase-space diagram. The expected ram pressure increases with the ICM density, which gets higher going towards the cluster centre, and with the square of the differential velocity, Δv_{cl}^2 (ref. 4). Thus, the most favourable conditions for ram pressure are at low radii and high Δv_{cl} (ref. 29), where most of our jellyfish galaxies are located (Fig. 4; see also Methods).

Thus, the phase-space diagram strongly supports the hypothesis that it is ram pressure that triggers the AGN, and not vice versa. If the AGN were making the ram-pressure efficiency anomalously high, there is no reason this should happen at the observed, most favourable location in the phase-space diagram. This does not exclude the possibility that the energy injected by the AGN contributes to efficient gas loss, and helps to create the spectacular tentacles we observe, with a sort of 'AGN feedback' in a cycle of ram pressure triggering AGN, which themselves favour ram pressure. Simulations of ram-pressure stripping including an AGN do not exist yet, but would be very valuable for interpreting our discovery.

Online Content Methods, along with any additional Extended Data display items and Source Data, are available in the online version of the paper; references unique to these sections appear only in the online paper.

Received 26 April; accepted 21 June 2017.

1. Krawczynski, H. & Treister, E. Active galactic nuclei the physics of individual sources and the cosmic history of formation and evolution. *Front. Phys.* **8,** 609–629 (2013).
2. Heckman, T. M. & Best, P. N. The coevolution of galaxies and supermassive black holes: insights from surveys of the contemporary universe. *Annu. Rev. Astron. Astrophys.* **52,** 589–660 (2014).
3. Boselli, A. & Gavazzi, G. Environmental effects on late-type galaxies in nearby clusters. *Publ. Astron. Soc. Pacif.* **118,** 517–559 (2006).
4. Gunn, J. E. & Gott, J. R. On the infall of matter into clusters of galaxies and some effects on their evolution. *Astrophys. J.* **176,** 1–19 (1972).
5. Fumagalli, M. *et al.* MUSE sneaks a peek at extreme ram-pressure stripping events — I. A kinematic study of the archetypal galaxy ESO137–001. *Mon. Not. R. Astron. Soc.* **445,** 4335–4344 (2014).
6. Ebeling, H. *et al.* Jellyfish: evidence of extreme ram-pressure stripping in massive galaxy clusters. *Astrophys. J.* **781,** L40–L44 (2014).
7. Magorrian, J. *et al.* The demography of massive dark objects in galaxy centers. *Astron. J.* **115,** 2285–2305 (1998).
8. Gültekin, K. *et al.* The M-σ and M-L relations in galactic bulges, and determinations of their intrinsic scatter. *Astrophys. J.* **698,** 198–221 (2009).
9. Sanders, D. *et al.* Ultraluminous infrared galaxies and the origin of quasars. *Astrophys. J.* **325,** 74–91 (1988).
10. Hopkins, P. & Hernquist, L. A characteristic division between the fueling of quasars and Seyferts: five simple tests. *Astrophys. J.* **694,** 599–609 (2009).
11. Moore, B. *et al.* Galaxy harassment and the evolution of clusters of galaxies. *Nature* **379,** 613–616 (1996).
12. White, S. D. M. & Rees, M. J. Core condensation in heavy halos — a two-stage theory for galaxy formation and clustering. *Mon. Not. R. Astron. Soc.* **183,** 341–358 (1978).
13. Bekki, K. & Couch, W. Starbursts from the strong compression of galactic molecular clouds due to the high pressure of the intracluster medium. *Astrophys. J.* **596,** L13–L16 (2003).
14. Poggianti, B. M. *et al.* Jellyfish galaxy candidates at low redshift. *Astron. J.* **151,** 78–97 (2016).

© 2017 Macmillan Publishers Limited, part of Springer Nature. All rights reserved.

15. Poggianti, B. M. *et al.* GASP I: Gas stripping phenomena in galaxies with MUSE. *Astrophys. J.* **844,** 48 (2017).
16. Bellhouse, C. *et al.* GASP II. A MUSE view of extreme ram-pressure stripping along the line of sight: kinematics of the jellyfish galaxy JO201. *Astrophys. J.* **844,** 49 (2017).
17. Gullieuszik, M. *et al.* GASP IV: A MUSE view of extreme ram-pressure stripping in the plane of the sky: the case of jellyfish galaxy JO204. Astrophys. J. (in the press).
18. Kewley, L. J. *et al.* Optical classification of southern warm infrared galaxies. *Astrophys. J. Suppl. Ser.* **132,** 37 (2001).
19. Kauffmann, G. *et al.* The host galaxies of active galactic nuclei. *Mon. Not. R. Astron. Soc.* **346,** 1055 (2003).
20. Sharp, R. G. & Bland-Hawthorn, J. Three-dimensional integral field observations of 10 galactic winds. I. Extended phase ($\geq$ 10 Myr) of mass/energy injection before the wind blows. *Astrophys. J.* **711,** 818 (2010).
21. Kewley, L. J. *et al.* The host galaxies and classification of active galactic nuclei. *Mon. Not. R. Astron. Soc.* **372,** 961–976 (2006).
22. Marziani, P. *et al.* Emission line galaxies and active galactic nuclei in WINGS clusters. *Astron. Astrophys.* **599,** A83 (2017).
23. Brinchmann, J. *et al.* The physical properties of star-forming galaxies in the low-redshift Universe. *Mon. Not. R. Astron. Soc.* **351,** 1151–1179 (2004).
24. Schulz, S. & Struck, C. Multi stage three-dimensional sweeping and annealing of disc galaxies in clusters. *Mon. Not. R. Astron. Soc.* **328,** 185–202 (2001).
25. Tonnesen, S. & Bryan, G. L. Gas stripping in simulated galaxies with a multiphase interstellar medium. *Astrophys. J.* **694,** 789–804 (2009).
26. Tonnesen, S. & Bryan, G. L. Star formation in ram pressure stripped galactic tails. *Mon. Not. R. Astron. Soc.* **422,** 1609–1624 (2012).
27. Ramos-Martinez, M. & Gomez, G. C. MHD simulations of ram pressure stripping of disk galaxies, in Galaxies at high redshift and their evolution over cosmic time. *IAU Symp.* **319,** 143–143 (2016).
28. Bower, R. *et al.* Breaking the hierarchy of galaxy formation. *Mon. Not. R. Astron. Soc.* **370,** 645–655 (2006).
29. Jaffé, Y. *et al.* BUDHIES II: a phase-space view of H I gas stripping and star formation quenching in cluster galaxies. *Mon. Not. R. Astron. Soc.* **448,** 1715–1728 (2015).
30. Navarro, J. F., Frenk, C. S. & White, S. D. M. A universal density profile from hierarchical clustering. *Astrophys. J.* **490,** 493–508 (1997).

Acknowledgements This work is based on observations collected at the European Organisation for Astronomical Research in the Southern Hemisphere under ESO programme 196.B-0578. We thank M. Fossati and D. Wilman for developing and making available KUBEVIZ. We acknowledge financial support from PRIN-INAF 2014. B.V. acknowledges support from an Australian Research Council Discovery Early Career Researcher Award (PD0028506). S.T. was supported by an Alvin E. Nashman Fellowship in Theoretical Astrophysics. This work was co-funded under the Marie Curie Actions of the European Commission (FP7-COFUND).

Author Contributions All authors contributed to the interpretation of the observations and the writing of the paper. B.M.P. led the project and performed the data analysis. Y.J. performed the phase-space analysis. A.M. carried out the stellar kinematics analysis. M.G. did the data reduction. M.R. contributed to the data analysis. S.T. provided the discussion on simulations. J.F. did the SINOPSIS analysis. D.B. and G.F. helped in the preparation of the observations. B.V. performed a comparison of the stellar population analysis and prepared the GASP web page. C.B. performed the two-component KUBEVIZ analysis of JO201. G.H. did the data reduction for JO201. A.O. selected the JW100 target.

Author Information Reprints and permissions information is available at www.nature.com/reprints. The authors declare no competing financial interests. Readers are welcome to comment on the online version of the paper. Publisher's note: Springer Nature remains neutral with regard to jurisdictional claims in published maps and institutional affiliations. Correspondence and requests for materials should be addressed to B.M.P. (bianca.poggianti@oapd.inaf.it).

© 2017 Macmillan Publishers Limited, part of Springer Nature. All rights reserved.

METHODS

In this work we adopt a standard concordance cosmology with a Hubble constant $H_0 = 70\,\mathrm{km\,s^{-1}\,Mpc^{-1}}$, the matter density $\Omega_M = 0.3$, and the vacuum energy density $\Omega_\Lambda = 0.7$ and a stellar initial mass function from ref. 31. The OmegaWINGS spectroscopic catalogue used to generate Fig. 4 is taken from ref. 32.

Observations and line fitting. The galaxies analysed in this Letter have been observed by the GASP program with 1 or 2 (depending on the length of the tentacles) MUSE pointings of 2,700 s each in service mode, with seeing conditions $\leq$1 arcsec. The MUSE spectrograph[33] has a $1' \times 1'$ field-of-view with $0.2'' \times 0.2''$ pixels with a spectral range 4,800–9,300 Å at 2.6 Å resolution. Before the analysis, the datacube is average-filtered in the spatial dimension with a 5×5 pixel kernel, corresponding to 1 arcsec (the upper limit of the seeing) = 0.8–1.1 kpc depending on the galaxy redshift. No smoothing or binning is performed in the spectral direction. The observations, data reduction and analysis tools are described in detail in ref. 15.

Emission lines in the datacube are fitted with Gaussian profiles with KUBEVIZ[34], a public IDL software that uses the MPfit package and provides gas velocities (with respect to a given redshift), velocity dispersions and line fluxes. KUBEVIZ can attempt a single or a double component fit (see ref. 16 for details). Three of the galaxies presented in this work—JO201, JO204 and JW100—require a double component fit, for which we have shown velocity and diagnostic diagrams for each of the two components separately. None of these galaxies have a broad component in permitted lines (Seyfert 1), with Hα widths (σ) up to a few hundred km s^{-1}.

In JO135, there is a small central region (white in Fig. 3) where a line Gaussian (even a double) fit cannot be obtained. Inspecting the MUSE spectra, it is clear that this is due to the very strong asymmetry of the lines, indicating a very powerful nuclear outflow. We note that the literature reports an 8 kpc AGN outflow in another jellyfish galaxy, NGC 4569 in the Virgo cluster[35].

The line intensities in Extended Data Fig. 1 are measured from KUBEVIZ in mask mode, masking out all the spaxels outside the region of interest (a spaxel is a pixel of integrated field spectroscopy, and corresponds to a specific position on the sky). In this case KUBEVIZ was run in interactive mode, to verify visually the quality of the fit. The error bars are computed propagating the KUBEVIZ errors on the line fluxes, and are small thanks to the very high signal-to-noise ratios of the spectra.

Analysis techniques. The results shown in Fig. 3 have been obtained from the datacube corrected both for Galactic extinction and for intrinsic dust extinction calculated from the Hα/Hβ ratio[15] and after having subtracted the stellar component using the spectrophotometric fits of the code SINOPSIS[36]. This code, fully described in ref. 36, searches the combination of single stellar population (SSP) spectra that best fits the observed equivalent widths of the main lines in absorption and in emission and the continuum at various wavelengths, minimizing the χ^2 using an Adaptive Simulated Annealing algorithm. The current version of SINOPSIS uses the latest SSP models (S. Charlot and G. Bruzual, manuscript in preparation) that have higher spectral and age resolution than previous versions and cover metallicity values from $Z = 0.0001$ to $Z = 0.04$. These models use the latest evolutionary tracks from ref. 37 and stellar atmosphere emission from a compilation of different authors. Moreover, SINOPSIS includes nebular emission for the youngest (that is, age $< 2 \times 10^7$ yr) SSP, computed by ingesting the original models into the plasma simulation code CLOUDY[38]. SINOPSIS provides spatially resolved maps of stellar masses, star-formation rates, star-formation histories, luminosity-weighted ages and other stellar population properties. The total galaxy stellar masses listed in Extended Data Table 1 are computed by summing up the stellar mass in each spaxel estimated from SINOPSIS.

The stellar kinematics are derived using the Penalized Pixel-Fitting code[39], with the method presented in ref. 15. This code fits the observed spectra with the stellar population templates from ref. 40, using SSPs of 6 different metallicities (from $[M/H] = -1.71$ to $[M/H] = 0.22$) and 26 ages, from 1 to 17.78 Gyr. After having accurately masked spurious sources (stars, background galaxies) in the galaxy proximity, and having degraded the spectral library resolution to our MUSE resolution, we performed the fit of spatially binned spectra based on signal-to-noise ratio ($S/N = 10$, for most galaxies), as described in ref. 41, with the Weighted Voronoi Tessellation modification proposed in ref. 42. This yields maps of the rotational velocity, the velocity dispersion and the two h3 and h4 moments using an additive Legendre polynomial fit of the 12th order to correct the template continuum shape during the fit.

The gas velocity map (Figs 1 and 2) is obtained from the absorption-corrected cube average filtering in the spatial directions with a 5×5 pixel kernel, plotting only spaxels with $S/N_{\mathrm{H}\alpha} > 4$. The stellar map is shown for the Voronoi bins with $S/N > 10$. We note that in Figs 1 and 2 the gaseous and stellar velocity zero points are coincident and correspond to the galaxy redshift listed in Extended Data Table 1, except for JW100 where the stellar zeropoint is at redshift $z = 0.06214$ because gas and stars have a large systematic shift. The contours in Figs 1 and 2 are logarithmically spaced isophotes of the spectral continuum underlying H$_\alpha$, thus are stellar isophotes, down to a surface brightness 2.5×10^{-18} erg s^{-1} cm^{-1} Å^{-1} arcsec^{-2}.

As mentioned above, LINER-like emission-line ratios (above the solid line and to the right of the dashed line in Extended Data Fig. 1) can originate from a variety of physical processes[43–46]. In constrast, the Seyfert-like line ratios (above the solid line and to the left of the dashed line in Extended Data Fig. 1) of JO201, JO204, JW100, JO206 and JO135 identify these galaxies as AGN. This conclusion is further strengthened by the equivalent widths of Hα and [O III]5,007 measured from the integrated spectra of the region powered by the AGN, whose rest-frame, absorption-corrected values, given in Extended Data Table 1, are higher than the low values measured in LINERs[46], typically EW(Hα) < 3 Å (EW, equivalent width).

Shocks induced by gas flows (in our case, by ram pressure) can give rise to line ratios that occupy also the 'AGN' locus in the diagnostic diagrams[47], however the spatial distribution of the AGN-dominated spaxels, at the galaxy centre, makes it very unlikely this is due to ram-pressure shocks (which would be observed at the shock fronts with the ICM), and strongly favours the AGN hypothesis.

The ram pressure can be computed[4] as $P_{\mathrm{ram}} = \rho_{\mathrm{ICM}} \times \Delta v_{\mathrm{cl}}^2$, where ρ_{ICM} is the ICM density and Δv_{cl}^2 is the differential galaxy velocity with respect to the cluster, as in Fig. 4. Figure 4 shows that most of our jellyfish galaxies are indeed in the conditions of strong ram pressure, being at very high (JO204, JO206, $|\Delta v_{\mathrm{cl}}|/\sigma_{\mathrm{cl}} > 1$) or extremely high (JO201, JW100 and JO194, $|\Delta v_{\mathrm{cl}}|/\sigma_{\mathrm{cl}} > 2.5$) velocities, and very small (projected) radii. JO135 is at a small projected cluster-centric radius, but its relative radial velocity is lower than the other AGN. However, its 3D velocity relative to the ICM might be much larger if the tangential velocity (along the plane of the sky) is much higher than the radial velocity, as suggested by Fig. 2. Moreover, JO135 is part of the Shapley supercluster and it is located at a position where the two clusters A3532 and A3530 are merging, and this probably causes a ram-pressure enhancement[48]. Interestingly, JO175, which is the only jellyfish galaxy with no evidence for an AGN, lies at low relative radial velocity, $|\Delta v_{\mathrm{cl}}|/\sigma_{\mathrm{cl}} \approx 0.3$.

Code availability. This work made use of the KUBEVIZ software, which is publicly available at http://www.mpe.mpg.de/~dwilman/kubeviz/, of the Voronoi binning and pPXF software available at http://www-astro.physics.ox.ac.uk/~mxc/software/, and the SINOPSIS code that is publicly available under the MIT open source licence and can be downloaded from http://www.crya.unam.mx/gente/j.fritz/JFhp/SINOPSIS.html

Data availability. The MUSE data that support the findings of this study are part of the Phase 3 data release of the GASP program and will be available in the ESO Archive at http://archive.eso.org/cms.html. The first GASP public data release, including the data regarding this article, will happen at the end of 2017.

31. Chabrier, G. Galactic stellar and substellar initial mass function. *Publ. Astron. Soc. Pacif.* **115,** 763–795 (2003).
32. Moretti, A. *et al.* OmegaWINGS: spectroscopy in the outskirts of local clusters of galaxies. *Astron. Astrophys.* **599,** A81 (2017).
33. Bacon, R. *et al.* The MUSE second-generation VLT instrument. *Proc. SPIE* **7735,** 773508 (2010).
34. Fossati, M. *et al.* MUSE sneaks a peek at extreme ram-pressure stripping events — II. The physical properties of the gas tail of ESO137-001. *Mon. Not. R. Astron. Soc.* **455,** 2028–2041 (2016).
35. Boselli, A. *et al.* Spectacular tails of ionized gas in the Virgo cluster galaxy NGC 4569. *Astron. Astrophys.* **587,** A68 (2016).
36. Fritz, J. *et al.* GASP III. JO36: a case of multiple environmental effects at play? Preprint at http://arXiv.org/abs/1704.05088 (2017).
37. Bressan, A. *et al.* PARSEC: stellar tracks and isochrones with the PAdova and TRieste Stellar Evolution Code. *Mon. Not. R. Astron. Soc.* **427,** 127–145 (2012).
38. Ferland, G. J. *et al.* The 2013 release of CLOUDY. *Rev. Mex. Astron. Astrofis.* **49,** 137–163 (2013).
39. Cappellari, M. & Emsellem, E. Parametric recovery of line-of-sight velocity distributions from absorption-line spectra of galaxies via penalized likelihood. *Publ. Astron. Soc. Pacif.* **116,** 138–147 (2004).
40. Vazdekis, A. *et al.* Evolutionary stellar population synthesis with MILES — I. The base models and a new line index system. *Mon. Not. R. Astron. Soc.* **404,** 1639–1671 (2010).
41. Cappellari, M. & Copin, Y. Adaptive spatial binning of integral-field spectroscopic data using Voronoi tessellations. *Mon. Not. R. Astron. Soc.* **342,** 345–354 (2003).
42. Diehl, S. & Statler, T. S. Adaptive binning of X-ray data with weighted Voronoi tessellations. *Mon. Not. R. Astron. Soc.* **368,** 497–510 (2006).
43. Sarzi, M. *et al.* The SAURON project — XVI. On the sources of ionization for the gas in elliptical and lenticular galaxies. *Mon. Not. R. Astron. Soc.* **402,** 2187–2210 (2010).
44. Yan, R. & Blanton, M. R. The nature of LINER-like emission in red galaxies. *Astrophys. J.* **747,** 61 (2012).
45. Singh, R. *et al.* The nature of LINER galaxies. Ubiquitous hot old stars and rare accreting black holes. *Astron. Astrophys.* **558,** A43 (2013).
46. Belfiore, F. *et al.* SDSS IV MaNGA — spatially resolved diagnostic diagrams: a proof that many galaxies are LIERs. *Mon. Not. R. Astron. Soc.* **461,** 3111–3134 (2016).

© 2017 Macmillan Publishers Limited, part of Springer Nature. All rights reserved.

47. Allen, M. G. *et al.* The MAPPINGS III library of fast radiative shock models. *Astrophys. J. Suppl. Ser.* **178,** 20–55 (2008).
48. Owers, M. *et al.* Shocking tails in the major merger Abell 2744. *Astrophys. J.* **750,** L23 (2012).
49. Cava, A. *et al.* WINGS-SPE spectroscopy in the WIde-field Nearby Galaxy-cluster Survey. *Astron. Astrophys.* **495,** 707–719 (2009).
50. Wang, S. *et al.* CHANDRA ACIS survey of X-ray point sources: the source catalog. *Astrophys. J. Suppl. Ser.* **224,** 40 (2016).

© 2017 Macmillan Publishers Limited, part of Springer Nature. All rights reserved.

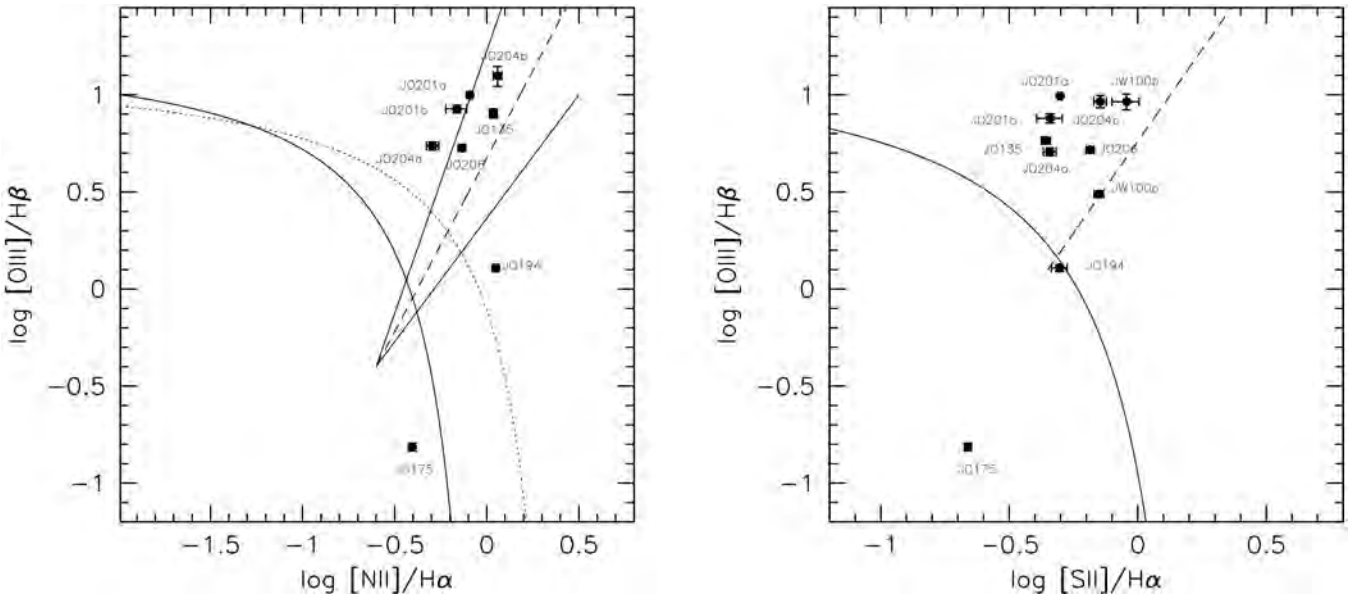

Extended Data Figure 1 | Summary diagnostic diagrams. Line ratio diagrams summarizing our findings, showing the location of each galaxy in two different diagnostics diagrams integrating the spectrum over the spatial region (identified from Fig. 3) dominated by AGN emission (JO201, JO204, JW100, JO206, JO135), by LINER emission (JO194) and over the central 7×7 brightest spaxels in the case of JO175. Here we present both the [N II]6,583/Hα (left) and the [S II]6,717/Hα (right) diagrams, to illustrate the good agreement between the two and also to display JW100 whose [N II] line cannot be measured. Lines as in Fig. 3. The two components in JO201, JO204 and JW100 are shown as separate points. The error bars are computed propagating the errors on the line fluxes obtained by KUBEVIZ, scaled to achieve a reduced $\chi^2 = 1$ as described elsewhere[15].

© 2017 Macmillan Publishers Limited, part of Springer Nature. All rights reserved.

Extended Data Table 1 | Properties of GASP jellyfish galaxies

ID_{P16}	ID_{WINGS}	cluster	σ_{cl} (km s^{-1})	RA	DEC	z	M_* ($M_\odot$)	L_X (erg s^{-1}, 0.3-8keV)	$L_{[OIII]}$ erg s^{-1}	EW(Hα) Å r.f.	EW([OIII]) Å r.f.
JO201	WINGSJ004130.30-091546.1	A85	982 ± 55	00 41 30.30	-09 15 45.98	0.04464	6.7×10^{10}	7.3×10^{41}	$1.37 \pm 0.03 \times 10^{42}$	46.0/14.4±1.0/0.9	141.8/44.2±6.1/2.6
JO204	WINGSJ101346.82-005450.9	A957	640 ± 47	10 13 46.84	-00 54 51.27	0.04243	4.4×10^{10}	–	$4.94 \pm 0.3 \times 10^{40}$	12.8/10.6±0.5/0.4	23.5/19.2± 1.2/1.1
JW100	WINGSJ233625.05+210902.5	A2626	679 ± 60	23 36 25.05	+21 09 02.64	0.06019	3.2×10^{11}	2.0×10^{41}	$2.16 \pm 0.06 \times 10^{40}$	5.6/2.6±0.2/0.3	4.1/4.0± 0.1/0.1
JO206	WINGSJ211347.41+022834.9	IIZW108	611 ± 38	21 13 47.41	+02 28 35.50	0.05133	1.1×10^{11}	7.7×10^{42}	$1.11 \pm 0.04 \times 10^{41}$	33.5±1.0	50.1±2.2
JO135	WINGSJ125704.29-302230.6	A3532	805 ± 61	12 57 04.32	-30 22 30.19	0.05421	1.0×10^{11}	3.2×10^{41}	$1.29 \pm 0.06 \times 10^{41}$	26.3±1.0	39.4±1.8
JO194	WINGSJ235700.68-344050.1	A4059	752 ± 38	23 57 00.74	-34 40 49.94	0.04100	1.6×10^{11}	1.4×10^{41}	$2.94 \pm 0.07 \times 10^{39}$	3.2±0.07	0.9±0.02
JO175	WINGSJ205117.58-524921.5	A3716	848 ± 26	20 51 17.59	-52.49 22.34	0.04678	3.9×10^{10}	–	–	43.9±0.9	1.4±0.08

From left to right, columns show the IDs of our galaxies (as given elsewhere[14]), their host cluster name, the cluster velocity dispersion[30,49], galaxy coordinates, redshifts, stellar masses, X-ray luminosities (from ref. 50), GASP [O III]5,007 luminosities and rest frame emission-only equivalent widths (EWs) of Hα and [O III]5,007. [O III]5,007 luminosities and EWs have been computed from the absorption-corrected integrated spectra of the AGN regions (LINER for JO194, and central star-forming region for JO175), see Extended Data Fig. 1. In the cases of galaxies with two components, the [O III] luminosity is the sum of the two luminosities and the two EWs are listed separated by a slash. The sum of these two EWs can be thought of as a 'total' EW. Other properties of these galaxies (gas and stellar kinematics, stellar history, gas metallicity and others) are the subject of dedicated publications[15–17].

© 2017 Macmillan Publishers Limited, part of Springer Nature. All rights reserved.